arXiv:2106.01908v2 [cs.CV] 2 Oct 2021

You Never Cluster Alone

Yuming Shen*[1], Ziyi Shen[2], Menghan Wang[3], Jie Qin[4], Philip H.S. Torr[1], and Ling Shao[5]

[1]University of Oxford [2]University College London [3]eBay
[4]Nanjing University of Aeronautics and Astronautics [5]Inception Institute of Artificial Intelligence

Abstract

Recent advances in self-supervised learning with instance-level contrastive objectives facilitate unsupervised clustering. However, a standalone datum is not perceiving the context of the holistic cluster, and may undergo sub-optimal assignment. In this paper, we extend the mainstream contrastive learning paradigm to a cluster-level scheme, where all the data subjected to the same cluster contribute to a unified representation that encodes the context of each data group. Contrastive learning with this representation then rewards the assignment of each datum. To implement this vision, we propose twin-contrast clustering (TCC). We define a set of categorical variables as clustering assignment confidence, which links the instance-level learning track with the cluster-level one. On one hand, with the corresponding assignment variables being the weight, a weighted aggregation along the data points implements the set representation of a cluster. We further propose heuristic cluster augmentation equivalents to enable cluster-level contrastive learning. On the other hand, we derive the evidence lower-bound of the instance-level contrastive objective with the assignments. By reparametrizing the assignment variables, TCC is trained end-to-end, requiring no alternating steps. Extensive experiments show that TCC outperforms the state-of-the-art on challenging benchmarks.

1 Introduction

Ancestored by various similarity-based [59] and feature-based [4, 56] approaches, unsupervised deep clustering jointly optimizes data representations and cluster assignments [81]. A recent fashion in this domain takes inspiration from contrastive learning in computer vision [11, 12, 24], leveraging the effectiveness and simplicity of discriminative feature learning. This strategy is experimentally reasonable, as previous research has found that the learnt representations reveal data semantics and locality [34, 80]. Even a simple migration of contrastive learning significantly improves clustering performance, of which examples include a two-stage clustering pipeline [73] with contrastive pre-training and k-means [56] and a composition of an InfoNCE loss [62] and a clustering one [81] in [89]. Compared with the deep generative counterparts [16, 36, 54, 86], contrastive clustering is free from decoding and computationally practical, with guaranteed feature quality.

However, have we been paying too much attention to the representation expressiveness of a single data point? Intuitively, a standalone data point, regardless of its feature quality, cannot tell us much about how the cluster looks like. Fig. 1 illustrates a simple analogy using the *TwoMoons* dataset. Without any context for the crescents, it is difficult to assign a data point to either of the two clusters based on its own representation, as the point can be inside one moon but still close to the other. Accordingly, observing more data reveals more about the holistic distributions of the clusters, *e.g.*, the shapes of the moons in Fig. 1, and thus heuristically benefits clustering. Although we can implicitly parametrize the context of the clusters by the model itself, *e.g.*, using a Gaussian mixture model (GMM) [4] or encoding this information by deep model parameters, explicitly representing the context yields the most common deep learning practice. This further opens the door for learning cluster-level representations with all corresponding data points. *Namely, you never cluster alone*.

*A part of this work was done when the author was with eBay.

35th Conference on Neural Information Processing Systems (NeurIPS 2021), Sydney, Australia.

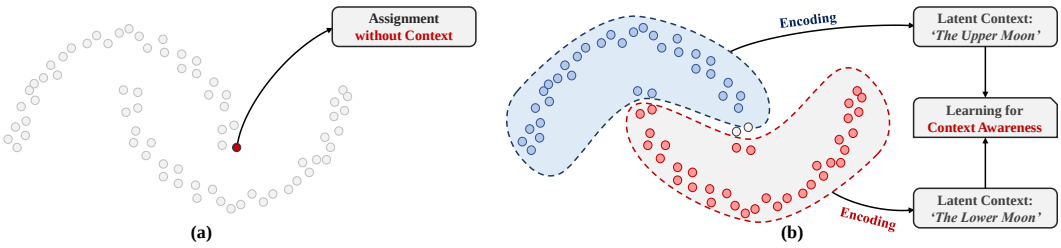


Figure 1: The motivation behind this work. **(a):** When assessing a standalone data point, cluster assignment can be challenging due to the non-linearity of the feature space and the lack of context information for the data distribution. **(b):** Our model learns this context by representing each cluster with latent features.

In this paper, motivated by the thought experiment above, we develop a multi-granularity contrastive learning framework, which includes an instance-level granularity and a cluster-level one. The former learning track conveys the conventional functionalities of contrastive learning, *i.e.*, learning compact data representations and preserving underlying semantics. We further introduce a set of latent variables as cluster assignments, and derive an evidence lower bound (ELBO) of instance-level InfoNCE [62]. As per the cluster-level granularity, we leverage these latent variables as weights to aggregate all the corresponding data representations as the set representation [87] of a cluster. We can then apply contrastive losses to all clusters, thereafter rewarding/updating the cluster assignments. Abbreviated as twin-contrast clustering (TCC), our work delivers the following contributions:

- We develop the novel TCC model, which, for the first time, shapes and leverages a unified representation of the cluster semantics in the context of contrastive clustering.
- We define and implement the cluster-level augmentations in a batch-based training and stochastic labelling procedure, which enables on-the-fly contrastive learning on clusters.
- We achieve significant performance gains against the state-of-the-art methods on five benchmark datasets. Moreover, TCC can be trained from scratch, requiring no pre-trained models or auxiliary knowledge from other domains.

2 Preliminaries

2.1 Contrastive Learning

Contrastive learning, as the name suggests, aims to distinguish an instance from all others using embeddings, with the dot-product similarity typically being used as the measurement. Let $\mathbf{X} = \{\mathbf{x}_i\}_{i=1}^N$ be an N-point dataset, with the i-th observation $\mathbf{x}_i \in \mathbb{R}^{d_x}$. An arbitrary transformation $f : \mathbb{R}^{d_x} \to \mathbb{R}^{d_m}$ encodes each data point into a d_m-dimensional vector. With the index i being the identifier, the InfoNCE loss [62] discriminates $\mathbf{x}_i$ from the others through a softmax-like likelihood:

$$\log p\left(i|\mathbf{x}_i\right) = \log \frac{\exp\left(\mathbf{v}_i^\intercal f(\mathbf{x}_i)/\tau\right)}{\sum_{j=1}^N \exp\left(\mathbf{v}_j^\intercal f(\mathbf{x}_i)/\tau\right)}. \tag{1}$$

A temperature hyperparameter τ controls the concentration level [26, 80]. $\mathbf{V} = \{\mathbf{v}_i\}_{i=1}^N$ refers to the vocabulary of the dataset, which is usually based on the data embeddings under different augmentations. As caching the entire $\mathbf{V}$ is not practical for large-scale training, existing works propose surrogates of Eq. (1), *e.g.*, replacing $\mathbf{V}$ with a memory bank [80], queuing it with a momentum network [12, 24], or training with large batches [11]. Following [24, 73], we slightly abuse the notification to use Eq. (1) to indicate the cross-entropy loss in implementation for simplicity.

2.2 Deep Set Representations

To learn the representations of sets, we need to consider permutation-invariant transformations. Zaheer *et al.* [87] showed that all permutation-invariant functions $T(\cdot)$ applied to a set $\mathbf{X}$ generally fall into the following form:

$$T(\mathbf{X}) = g\left(\sum\nolimits_{i=1}^N h(\mathbf{x}_i)\right), \tag{2}$$

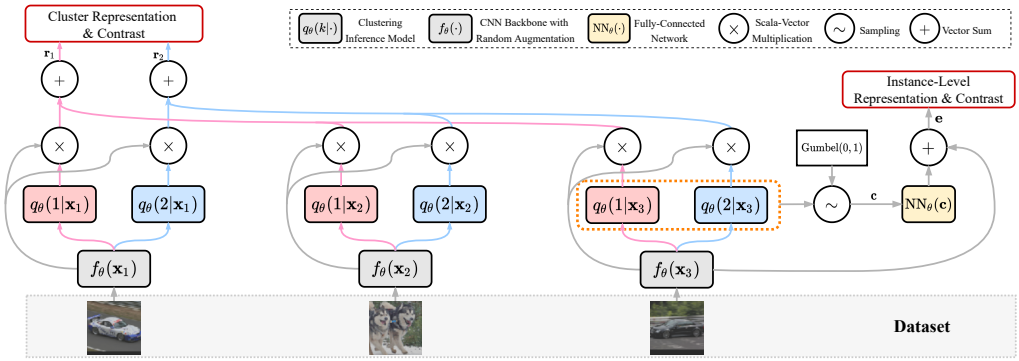


Figure 2: The schematic of TCC. Here, we demonstrate a 2-way clustering example with three images. For simplicity, we only illustrate the instance-level learning module on the last image, while it is applied to all images.

where $g(\cdot)$ and $h(\cdot)$ are arbitrary continuous transformations. Note that the aggregation above can be executed on a weighted basis, which is typically achieved by the attention mechanism between the set-level queries and instance-level keys/values [31, 49]. Our design on each cluster is partially inspired by this, as back-propagation does not support hard instance-level assignment. Next, we define our cluster representation along with the clustering procedure, and describe how it is trained with contrastive learning.

3 Twin-Contrast Clustering

We consider a K-way clustering problem, with K being the number of clusters. Let $k \in \{1, \cdots, K\}$ denote the entry of a cluster that $\mathbf{x}_i$ may belong to, and the categorical variable $\boldsymbol{\pi}_i = [\pi_i(1), \cdots, \pi_i(K)]$ indicate the cluster assignment probabilities of $\mathbf{x}_i$. Following common practice, we regard image clustering as our target for simplicity. Fig. 2 provides a schematic of TCC. The cluster-level contrast track reflects our motivation from Sec. 1, while the instance-level one learns the semantics of each image. We bridge these two tracks with the inference model $\pi_i(k) = q_\theta(k|\mathbf{x}_i)$ so that both losses reward and update the assignment on each $\mathbf{x}_i$. In particular, $q_\theta(k|\mathbf{x}_i)$ is parametrized by a softmax operation:

$$\pi_i(k) = q_\theta(k|\mathbf{x}_i) = \frac{\exp(\mu_k^\intercal f_\theta(\mathbf{x}_i))}{\sum_{k'=1}^{K} \exp(\mu_{k'}^\intercal f_\theta(\mathbf{x}_i))}, \tag{3}$$

where $f_\theta(\cdot)$ is a convolutional neural network (CNN) [47, 48] built upon random data augmentations, producing d_m-dimensional features. We denote $\boldsymbol{\mu}_\theta = \{\mu_k\}_{k=1}^K$ as a set of trainable cluster prototypes, where θ refers to the collection of all parameters. In Sec. 3.1, we leverage $q_\theta(k|\mathbf{x}_i)$ to aggregate cluster features, and in Sec. 3.2 we derive the ELBO of Eq. (1) with $q_\theta(k|\mathbf{x}_i)$. In the following, we will omit the index i for brevity when $\mathbf{x}$ and $\boldsymbol{\pi}$ clearly correspond to a single data point.

3.1 Representing and Augmenting the Context for Cluster-Level Contrast

Cluster-Level Representation We implement Eq. (2) for each cluster using soft aggregation, where $q_\theta(k|\mathbf{x})$ weighs the relevance of the data to the given cluster. Denoted as $\mathbf{r}_k$, the k-th cluster representation is computed by:

$$\begin{aligned} h_\theta(\mathbf{x}; k) &= \pi(k) \cdot f_\theta(\mathbf{x}), \\ \mathbf{r}_k = T_\theta(\mathbf{X}; k) &= \left(\sum_{i=1}^{N} h_\theta(\mathbf{x}_i; k)\right) \Big/ \left\| \sum_{i=1}^{N} h_\theta(\mathbf{x}_i; k) \right\|_2, \end{aligned} \tag{4}$$

where $\|\cdot\|_2$ refers to the L2-norm. We adopt L2 normalization here for two main purposes. First, the summation of $\pi(k) = q_\theta(k|\mathbf{x})$ along $\mathbf{x}$ is not self-normalized. Second, and more importantly, as shown in [11, 12, 24], L2-normalized features benefit contrastive learning.

The Anchored Cluster Semantics Intuitively, $\pi(k)$ reflects the degree of relevance of a datum to the k-th cluster. With it being the aggregation weight, $\mathbf{r}_k$ represents the information that is related to the corresponding prototype μ_k. In other words, our design treats each μ_k as the semantic anchor that queries the in-coming batch to form a representation describing a certain latent topic.

Cluster-Level Augmentation Equivalents Contrastive learning is usually employed alongside random data augmentation [11, 24] to obtain positive candidates. Though defining a uniform augmentation scheme for sets is beyond the scope of this paper, the proposed model reflects cluster-level augmentation in its design by the following heuristics:

(a) **Augmentation on elements.** TCC implicitly inherits existing image augmentation techniques (such as cropping, color jittering, random flipping, and grayscale conversion) by implementing them using $f_\theta(\cdot)$.

(b) **Irrelevant minorities.** We consider injecting a small proportion of irrelevant data into a cluster representation, while keeping the main semantics of the cluster unchanged. Eq. (4) turns out to be an equivalent to this. As the softmax product $\pi(k)$ is always positive, those data that are not very related to the given cluster still contribute to the cluster's representation, which compiles the **irrelevant**. Meanwhile, these irrelevant data are not dominating the value of the cluster representation, because the small value of $\pi(k)$ scales the feature magnitude during aggregation, which counts the **minority**.

(c) **Subsetting.** Empirically, a subset of a cluster holds the same semantics as the original. Batch-based training samples data at each step, which naturally creates subsets for each cluster.

We experimentally find the above augmentation equivalents are sufficient for the clustering task. On the other hand, since Eq. (4) is permutation-invariant, reordering the sequence of data does not yield a valid augmentation.

Cluster-Level Contrastive Learning We define a simple contrastive objective that preserves the identity of each cluster against the rest. Having everything in a batch, *e.g.*, a SimCLR-like framework [11], does not allow augmentation (c) to be fully utilized in the loss, since the two augmented counterparts $\mathbf{r}_k$ and $\hat{\mathbf{r}}_k$ from a batch may form part of the same subset of a cluster. Hence, we opt for the MoCo-like solution [24], employing an L-sized memory queue $\mathbf{P} = \{\mathbf{p}_l\}_{l=1}^{L}$ to cache negative samples and a momentum network to produce $\hat{\mathbf{r}}_k = T_{\hat{\theta}}(\mathbf{X}; k)$. $\mathbf{P}$ stores each cluster representation under different subsets, training with which preserves the temporal semantic consistency [45] of clusters. Our cluster-level objective minimizes the following negative log-likelihood (NLL):

$$\mathcal{L}_1 = \mathbb{E}_k[-\log\, p_\theta(k|\mathbf{r}_k)] = -\frac{1}{K}\sum_{k=1}^{K}\log\frac{\exp(\hat{\mathbf{r}}_k^\intercal \mathbf{r}_k/\tau)}{\exp(\hat{\mathbf{r}}_k^\intercal \mathbf{r}_k/\tau) + \sum_{l=1}^{L}\exp(\mathbf{p}_l^\intercal \mathbf{r}_k/\tau)\mathbb{1}(l \bmod K \neq k)}, \tag{5}$$

where $\mathbb{1}(\cdot)$ is an indicator function and $\bmod$ is the modular operator. Since the cluster number K can be less than the queue size L, we exclude the features that represent the same cluster as k in the negative sample collection $\mathbf{P}$ by inserting the indicator function into the loss above.

3.2 Instance-Level Contrast with Cluster Assignments

The ELBO We propose to reuse the inference model $q_\theta(k|\mathbf{x})$ discussed above to compute the instance-level contrastive loss, so that the clustering process can benefit from contrastive learning. Let us start from the following ELBO of $\log p_\theta(i|\mathbf{x})$ in Eq. (1):

$$\log p_\theta(i|\mathbf{x}) \geq \mathbb{E}_{q_\theta(k|\mathbf{x})}\left[\log p_\theta(i|\mathbf{x}, k)\right] - \mathrm{KL}\left(q_\theta(k|\mathbf{x})||p_\theta(k|\mathbf{x})\right), \tag{6}$$

where $\mathrm{KL}(\cdot)$ is the Kullback–Leibler (KL) divergence. We derive this ELBO in Appendix A. The true distribution $p_\theta(k|\mathbf{x})$ is not available under the unsupervised setting. We follow [40, 69] and use a fixed prior instead. In practice, we employ the uniform distribution, *i.e.*, $p_\theta(k|\mathbf{x}) \coloneqq p_\theta(k) = 1/K$. Then, the KL term above can be reduced to a simple form $-\mathrm{KL}\left(q_\theta(k|\mathbf{x})||p_\theta(k|\mathbf{x})\right) = \log K + \mathcal{H}(q_\theta(k|\mathbf{x}))$. Empirically, this encourages an evenly distributed cluster assignment across the dataset.

Regarding the expectation term in Eq. (6), back-propagation through the discrete entry k is not feasible. We resort to the Gumbel softmax trick [32, 57] as relaxation. Specifically, a latent variable $\mathbf{c} \in (0, 1)^K$ is assigned to each $\mathbf{x}$ as a replacement. Each entry $\mathbf{c}(k)$ yields the reparametrization $\mathbf{c}(k) = \mathrm{Softmax}_k((\log \pi(k) + \epsilon(k))/\lambda)$, where $\epsilon \sim \mathrm{Gumbel}(0, 1)$ and λ is another temperature hyperparameter. Hence, we obtain the surrogate $\mathbb{E}_{q_\theta(k|\mathbf{x})}\left[\log p_\theta(i|\mathbf{x}, k)\right] \simeq \mathbb{E}_\epsilon\left[\log p_\theta(i|\mathbf{x}, \mathbf{c})\right]$ and the gradients can be estimated with Monte Carlo.

Instance-Level Contrastive Learning In alignment with Eq. (5), $\log p_\theta(i|\mathbf{x}, \mathbf{c})$ learns the representation of $\mathbf{x}$ on a momentum contrast basis [24] by defining the following transformation:

$$\begin{aligned} \mathbf{e} &= (f_\theta(\mathbf{x}) + \mathrm{NN}_\theta(\mathbf{c}))/\|f_\theta(\mathbf{x}) + \mathrm{NN}_\theta(\mathbf{c})\|_2, \\ \log p_\theta(i|\mathbf{x}, \mathbf{c}) &= \log \frac{\exp(\hat{\mathbf{e}}^\intercal \mathbf{e}/\tau)}{\exp(\hat{\mathbf{e}}^\intercal \mathbf{e}/\tau) + \sum_{j=1}^{J} \exp(\mathbf{q}_j^\intercal \mathbf{e}/\tau)}, \end{aligned} \tag{7}$$

where $\mathrm{NN}_\theta(\cdot)$ denotes a single fully connected network. We accordingly use $\hat{\mathbf{e}}$ to indicate the representation of $\mathbf{x}$ processed by a momentum network $f_{\hat{\theta}}(\cdot)$ and $\mathrm{NN}_{\hat{\theta}}(\cdot)$ under different augmentations and Gumbel samplings [32, 57]. A J-sized memory queue $\mathbf{Q} = \{\mathbf{q}_j\}_{j=1}^{J}$ is also introduced to cache negative samples, updated by $\hat{\mathbf{e}}$. In this way, we obtain the instance-level loss:

$$\mathcal{L}_2 = \mathbb{E}_i[-\mathbb{E}_{\epsilon_i}[\log p_\theta(i|\mathbf{x}_i, \mathbf{c}_i)] - \mathcal{H}(q_\theta(k|\mathbf{x}_i)) - \log K]. \tag{8}$$

3.3 Training and Inference

TCC enables end-to-end training from scratch. Our learning objective is a simple convex combination of Eq. (5) and (8), *i.e.*,

$$\mathcal{L} = \alpha\mathcal{L}_1 + (1-\alpha)\mathcal{L}_2. \tag{9}$$

The hyperparameter $\alpha \in (0, 1)$ controls the contributions of the two contrastive learning tracks. As discussed in Sec. 3.1, $\mathcal{L}$ is computed following a batch-based routine. For each data point $\mathbf{x}$, we obtain only one sample $\mathbf{c}$ from the Gumbel distribution at each step, since this is usually sufficient for long-term training [39, 40, 69]. One may also regard this stochasticity as an alternative to data augmentation. The overall training algorithm is shown in Alg. 1. Here, $\mathbf{\Gamma}(\cdot)$ indicates an arbitrary stochastic gradient descent (SGD) optimizer.

Algorithm 1: Training Algorithm of TCC

Input: Dataset $\mathbf{X} = \{\mathbf{x}_i\}_{i=1}^{N}$
Output: Network parameters θ.
Initialize $\hat{\theta} = \theta$
repeat
  Randomly select a mini-batch from $\mathbf{X}$
  for *each* $\mathbf{x}_i$ *in the batch* **do**
    Randomly augment $\mathbf{x}_i$ twice
    Sample $\mathbf{c}_i$ with Gumbel softmax
  end
  $\mathcal{L} \leftarrow$ Eq. (9)
  $\theta \leftarrow \theta - \mathbf{\Gamma}(\nabla_\theta \mathcal{L})$
  Update the queues $\mathbf{P}$ with $\hat{\mathbf{r}}$ and $\mathbf{Q}$ with $\hat{\mathbf{e}}$
  Update $\hat{\theta}$ with momentum moving average
until *convergence or reaching max iteration*;

All trainable components are subscripted by θ, while those marked with $\hat{\theta}$ are the network momentum counterparts to be updated with momentum moving average. Inference with TCC only requires disabling random data augmentation and then computing $\mathrm{argmax}_k\, q_\theta(k|\mathbf{x})$.

Complexity When sampling once for each $\mathbf{x}$ during training, the time complexity for Eq. (9) is $\mathcal{O}(L+J)$, while the memory complexity for the memory bank turns out to be the same. Here we omit the complexity introduced by the CNN backbone and dot-product computation, as it is orthogonal to the design. Compared with the recent mixture-of-expert approach [73], which requires a time and memory complexity of $\mathcal{O}(KJ)$, TCC is trained in a more efficient way.

3.4 Relations to Existing Works

MiCE [73] also proposes a lower bound for the instance-level contrastive objective. However, it does not directly *reparametrize* the variational model $q_\theta(k|\mathbf{x})$ for lower-bound computation and inference, but instead employs a K-expert solution with EM. This design is less efficient than TCC since each data point needs to be processed by all K experts. Moreover, MiCE [73] does not consider cluster-level discriminability. SCL [28] follows a similar motivation to TCC in cluster-level discriminability, but it implements this with an instance-to-set similarity, while our model learns a unified representation for each cluster. Furthermore, in SCL [28], the clustering inference model is disentangled from the instance-level contrastive objective. In contrast, the inference model $q_\theta(k|\mathbf{x})$ of TCC contributes to instance-level discrimination (Eq. (6)).

We recently find CC [53] comes with a cluster-level contrastive loss as well. It utilizes the in-batch inference results $[\pi_1(k), \cdots, \pi_n(k)]$ to describe the k-th cluster. However, this procedure is not literally learning the cluster representation, since it is not permutation free. Re-ordering the batch may shift the semantics of the produced feature. We mitigate this issue with deep sets [87] and the empirical cluster-level augmentations for temporal consistency [45]. A similar problem is witnessed in [66]. In addition, our instance-level discrimination model yields a more general case than the one

of CC [53]. When removing the stochasticity and enforcing $p_\theta(i|\mathbf{x}, \mathbf{c}) \coloneqq p_\theta(i|\mathbf{c})$ in our model, $\mathcal{L}_2$ reduces to the one of [53]. We experimentally show that our design preserves more data semantics, and thus benefits clustering. Being not related to our main contribution, we provide more elaboration on this in Appendix B under the framework of variational information bottleneck [2].

4 Related Work

Deep Clustering In addition to the classic approaches [4, 13, 18, 20, 43, 56, 59, 78, 91], the concept of simultaneous feature learning and clustering with deep models can be traced back to [81, 83]. The successors, including [9, 23, 61, 68, 77, 79, 85], have continuously improved the performance since. As a conventional option for unsupervised learning, deep generative models are also widely adopted in clustering [10, 16, 35, 36, 42, 51, 58, 86, 90], usually backboned by VAE [39] and GAN [21]. However, generators are computationally expensive for end-to-end training, and often less effective than the discriminative models [15, 27, 33] in feature learning [11]. Recent research has considered contrastive learning in clustering [28, 53, 73, 74, 89]. We discuss the drawback of them and their relations to TCC in Sec. 3.4.

Contrastive Learning Contrastive learning learns compact image representations in a self-supervised manner [11, 12, 24, 62, 72]. There are various applications for this paradigm [34, 41, 82, 93]. We note that several contrastive learning approaches [7, 52] conceptually involve a clustering procedure. Nevertheless, they are based on a unified pre-training framework to benefit the downstream tasks, instead of delivering a specific clustering model.

Set Representations Our cluster-level representation (Eq. (4)) is a realization of deep sets [17, 87]. Existing research in this area mainly focuses on set-level tasks [19, 31, 37, 76, 84]. It is also notable that, though we leverage cluster-level representation learning, TCC is still an instance-level clustering model, which is different from the set-level clustering models [49, 50, 63].

5 Experiments

5.1 Settings

We follow the recent works [29, 33] and report the performance of TCC in terms of clustering accuracy (ACC) [81], normalized mutual information (NMI) [70] and adjusted random index (ARI) [30]. For fair comparison with existing works, we do not use any supervised pre-trained models. The experiments are conducted on five benchmark datasets, including CIFAR-10/100 [44], ImageNet-10/Dog [9] and STL-10 [14]. Note that ImageNet-10/Dog [9] is a subset of the original ImageNet dataset [67]. Since most existing works have pre-defined cluster numbers, we adopt this practice and follow their training/test protocols [29, 33, 61, 73]. Tab. 1 depicts the details of the settings.

Table 1: Dataset settings for our experiments.

Dataset	Images	Clusters (K)	Input Size
CIFAR-10 [44]	60,000	10	32×32
CIFAR-100 [44]	60,000	20	32×32
STL-10 [14]	13,000	10	96×96
ImageNet-10 [9]	13,000	10	96×96
ImageNet-Dog [9]	19,500	15	96×96

5.2 Implementation Details

TCC is implemented with the deep learning toolbox TensorFlow [1]. We choose the MoCo-style random image augmentations [24] for fair comparison with the recent works [28, 73]. We further link our choice of augmentations with the cluster representation temporal consistency in Sec. 3.1. Specifically, each image is successively processed by random cropping, gray-scaling, color jittering, and horizontal flipping, followed by mean-std standardization. We refer to [24, 73] for more details. We employ ResNet-34 [25] as the default CNN backbone $f_\theta(\cdot)$, which is also identical to [28, 73]. Appendix C gives a full illustration of the CNN structure. The image size d_x and cluster number K are fixed for each dataset, as shown in Tab. 1. The feature dimensionality is identical to the ResNet [25] output after global pooling, *i.e.*, $d_m = 128$. Following common practice [12, 24, 11], we fix the contrastive temperature $\tau = 1$, while using a slightly lower $\lambda = 0.8$ for the Gumbel softmax trick [32, 57] to encourage concrete assignments. We implement a fixed-length instance-level memory bank $\mathbf{Q}$ with a size of $J = 12,800$ to match up with the smallest dataset in our experiments. The size of the cluster-level memory bank $\mathbf{P}$ is set to $L = 100 \times K$, varying from each dataset. We have $\alpha = 0.5$ so that $\mathcal{L}_1$ and $\mathcal{L}_2$ provide equal contributions to training. The choice of batch size is

Table 2: Unsupervised clustering performance comparison with existing methods (in percentage %). We provide additional results on Tiny ImageNet [46] and comparison with more contrastive baselines such as SwAV [7] in Appendix D.

Method	CIFAR-10			CIFAR-100			STL-10			ImageNet-10			ImageNet-Dog		
	NMI	ACC	ARI	NMI	ACC	ARI	NMI	ACC	ARI	NMI	ACC	ARI	NMI	ACC	ARI
AC [22]	10.5	22.8	6.5	9.8	13.8	3.4	23.9	33.2	14.0	13.8	24.2	6.7	3.7	13.9	2.1
NMF [5]	8.1	19.0	3.4	7.9	11.8	2.6	9.6	18.0	4.6	13.2	23.0	6.5	4.4	11.8	1.6
AE [3]	23.9	31.4	16.9	10.0	16.5	4.8	25.0	30.3	16.1	21.0	31.7	15.2	10.4	18.5	7.3
DAE [75]	25.1	29.7	16.3	11.1	15.1	4.6	22.4	30.2	15.2	20.6	30.4	13.8	10.4	19.0	7.8
DCGAN [65]	26.5	31.5	17.6	12.0	15.1	4.5	21.0	29.8	13.9	22.5	34.6	15.7	12.1	17.4	7.8
DeCNN [88]	24.0	28.2	17.4	9.2	13.3	3.8	22.7	29.9	16.2	18.6	31.3	14.2	9.8	17.5	7.3
VAE [39]	24.5	29.1	16.7	10.8	15.2	4.0	20.0	28.2	14.6	19.3	33.4	16.8	10.7	17.9	7.9
JULE [85]	19.2	27.2	13.8	10.3	13.7	3.3	18.2	27.7	16.4	17.5	30.0	13.8	5.4	13.8	2.8
DEC [81]	25.7	30.1	16.1	13.6	18.5	5.0	27.6	35.9	18.6	28.2	38.1	20.3	12.2	19.5	7.9
DAC [9]	39.6	52.2	30.6	18.5	23.8	8.8	36.6	47.0	25.7	39.4	52.7	30.2	21.9	27.5	11.1
ADC [23]	-	32.5	-	-	16.0	-	-	53.0	-	-	-	-	-	-	-
DDC [8]	42.4	52.4	32.9	-	-	-	37.1	48.9	26.7	43.3	57.7	34.5	-	-	-
DCCM [79]	49.6	62.3	40.8	28.5	32.7	17.3	37.6	48.2	26.2	60.8	71.0	55.5	32.1	38.3	18.2
IIC [33]	51.3	61.7	41.1	-	25.7	-	43.1	49.9	29.5	-	-	-	-	-	-
MMDC [68]	57.2	70.0	-	25.9	31.2	-	49.8	61.1	-	71.9	81.1	-	27.4	11.9	-
PICA [29]	56.1	64.5	46.7	29.6	32.2	15.9	-	-	-	78.2	85.0	73.3	33.6	32.4	17.9
DCCS [92]	56.9	65.6	46.9	-	-	-	37.6	48.2	26.2	60.8	71.0	55.5	-	-	-
DHOG [15]	58.5	66.6	49.2	25.8	26.1	11.8	41.3	48.3	27.2	-	-	-	-	-	-
GATCluster [61]	47.5	61.0	40.2	21.5	28.1	11.6	44.6	58.3	36.3	59.4	73.9	55.2	28.1	32.2	16.3
IDFD [71]	71.4	81.5	66.3	42.6	42.5	26.4	64.3	75.6	57.5	**89.8**	**95.4**	**90.1**	54.6	59.1	41.3
CC [53]	70.5	79.0	63.7	43.1	42.9	26.6	**76.4**	**85.0**	**72.6**	85.9	89.3	82.2	44.5	42.9	27.4
MoCo baseline [73]	66.9	77.6	60.8	39.0	39.7	24.2	61.5	72.8	52.4	-	-	-	34.7	33.8	19.7
MiCE [73]	73.7	83.5	69.8	43.6	44.0	28.0	63.5	75.2	57.5	-	-	-	42.3	43.9	28.6
TCC	**79.0**	**90.6**	**73.3**	**47.9**	**49.1**	**31.2**	73.2	81.4	68.9	84.8	89.7	82.5	**55.4**	**59.5**	**41.7**

of importance to TCC in computing the cluster-level representations. We set it to $32 \times K$ by default to ensure that sufficient images can be assigned to a cluster at each step. Training TCC only requires SGD *w.r.t.* θ and momentum update *w.r.t.* $\hat{\theta}$. We employ the Adam optimizer [38] with a default learning rate of 3×10^{-3}, without learning rate scheduling. The momentum network is updated by $\hat{\theta} \leftarrow 0.999\hat{\theta} + 0.001\theta$, where all modules subscripted by $\hat{\theta}$ are involved in this procedure. We train TCC for at least $1,000$ epochs on a single NVIDIA V100 GPU.

5.3 Comparison with the State-of-the-Art

Baselines Both deep clustering and traditional models are compared, including a MoCO-based two-stage baseline introduced by [73]. Similar to the recent works [29, 33, 73, 79], we pick deep models that enable training from scratch and do not require supervised pre-training parameters, for fair and reasonable comparison. For this reason, baselines such as VaDE [36] and SPICE [60] are not included here. We also exclude the clustering refinement approaches [64] from our comparison as they are orthogonal to our design.

Results The clustering performance (in percentage %) is shown in Tab. 2. For those baselines that are not designed for clustering [3, 21, 39], we report the results with k-means on the produced features. TCC outperforms existing works on most benchmarks. In particular, on CIFAR-10 [44], TCC outperforms the state-of-the-art methods by large margins, *e.g.*, 7% higher in ACC than the second best one (*i.e.*, MiCE [73] with even stronger augmentations [11]). As a closely-related work, MiCE [73] only considers instance-level representation learning. The performance gain of TCC over MiCE endorses our motivation to introduce cluster-level representations. We also observe that TCC underperforms [53] on STL-10 [14] due to the exceptionally high performance of it on this dataset. However, TCC is still the runner-up on this dataset by a significant margin, and is superior to [53] on the other four datasets. We argue that the performance on larger datasets is of more importance when comparing contrastive deep clustering methods, as contrastive learning is originally designed for large-scale tasks. Fig. 3 illustrates the t-SNE [55] scattering results of TCC on CIFAR-10 [44] and STL-10 [14].

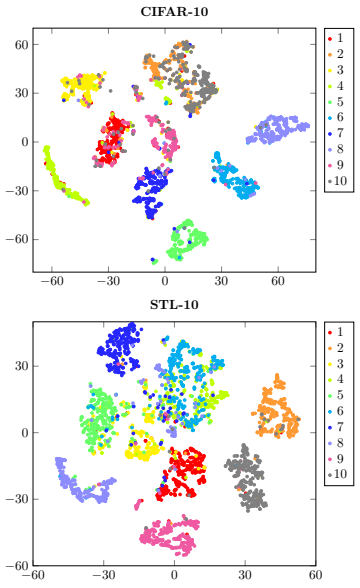


Figure 3: t-SNE visualization on CIFAR-10 [44] and STL-10 [14].

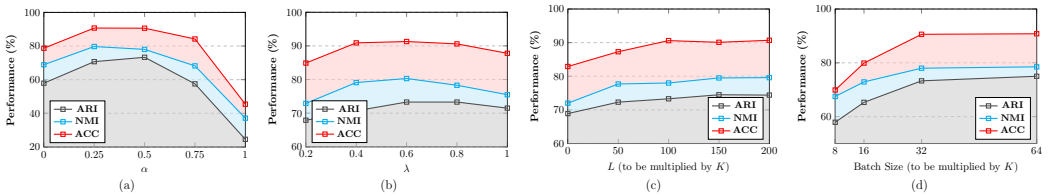


Figure 4: Hyperparameter analysis results on CIFAR-10 [44].

5.4 Ablation Study

We conduct an ablation study to validate our motivation and design, with the following baselines.

(i) **Without $\mathcal{L}_1$.** As a key component of TCC, the cluster-level contrastive learning objective $\mathcal{L}_1$ reflects our main motivation. We first assess the model performance when removing this loss, which reduces TCC to a simple instance-level contrastive clustering model.

(ii) **Without $\mathcal{L}_2$.** We can also remove $\mathcal{L}_2$ to see if $\mathcal{L}_1$ alone still yields a valid baseline.

(iii) **Multiple Sampling.** As described in Sec. 3.3, we only consider a single sample $\mathbf{c}$ each time to compute the lower bound of the instance-level loss (Eq. (8)). We also consider applying the Gumbel softmax trick multiple times for each image. In particular, we sample 10 groups of latent variables each time to compute the expectation term $\mathbb{E}_\epsilon \left[\log p_\theta(i|\mathbf{x}, \mathbf{c})\right]$ of $\mathcal{L}_2$. On each batch, we enqueue the mean of $\hat{\mathbf{c}}$ *w.r.t.* all 10 sampled $\mathbf{c}$ for each image.

(iv) **Without $\mathbf{P}$.** Since we usually have a small cluster number K, computing the cluster-level InfoNCE loss does not necessarily require a memory bank to cache the negative sample surrogates. In this baseline, we remove the cluster-level memory bank $\mathbf{P}$, and use the remaining $K-1$ cluster representations as negative samples when computing Eq. (5).

(v) **Without Augmentation (a) for $\mathcal{L}_1$.** We validate our cluster-level augmentation strategies by removing image augmentations when computing Eq. (8). Note that this baseline does not influence the instance-level objective by rendering both augmented and original images to $f_\theta(\cdot)$.

(vi) **Without Augmentation (b) for $\mathcal{L}_1$.** This baseline requires hard assignments at each step so that cluster-level aggregation only involves images that are assigned to the corresponding clusters. This modification does not affect $\mathcal{L}_2$.

(vii) **Without Augmentation (c) for $\mathcal{L}_1$.** The final baseline changes the training pipeline. Since we do not subset any clusters here, cluster representation aggregation (Eq. (4)) runs on the whole training set after each epoch. We apply alternating training procedure as follows. First, $\mathcal{L}_2$ optimizes the model for a full epoch. Then, we descend $\mathcal{L}_1$ with aggregated cluster features and repeat.

Table 3: Ablation study results (in percentage %).

	Baseline	CIFAR-10		
		NMI	ACC	ARI
(i)	Without $\mathcal{L}_1$	68.9	78.7	57.9
(ii)	Without $\mathcal{L}_2$	37.1	45.4	24.5
(iii)	Multiple Sampling	78.5	90.1	74.2
(iv)	Without $\mathbf{P}$	72.0	82.9	68.8
(v)	Without Augmentation (a) for $\mathcal{L}_1$	73.5	85.3	69.1
(vi)	Without Augmentation (b) for $\mathcal{L}_1$	68.5	79.2	60.6
(vii)	Without Augmentation (c) for $\mathcal{L}_1$	69.4	80.0	62.7
	TCC Full Model	79.0	90.6	73.3

Baseline Comparison Results We show the ablation study results in Tab. 3. Without $\mathcal{L}_1$, TCC performs similarly to the two-stage baseline with MoCo [24] and k-means [56] reported in [73], which is slightly lower than MiCE [73]. Interestingly, $\mathcal{L}_1$ does not provide instance-level discriminative information. Although it does still serve as a valid baseline, it does not perform very well (Baseline (ii)). Specifically, we experience strong degeneracy [6, 33] with this baseline, but it still produces better results than the traditional models. We also observe that having multiple samples with the Gumbel softmax trick [32, 57] for gradient estimation does not make much difference from a single-sample solution. Baseline (iv) also underperforms the original model. As discussed in previous sections, having a memory bank for cluster representations provides a way to acquire more negative samples for contrastive learning, considering the fact that the cluster number is usually limited.

Hyperparameters We evaluate the hyperparameters most essential to our design, including the loss weight α, the temperature of the Gumbel softmax λ, the cluster-level memory queue length L, and the batch size. The InfoNCE temperature τ and the instance-level memory queue length J are not included here since they are not relevant to our key motivation and have been employed and evaluated in the recent works [24, 28, 73]. The corresponding results are plotted in Fig. 4. Though $\mathcal{L}_1$ plays an

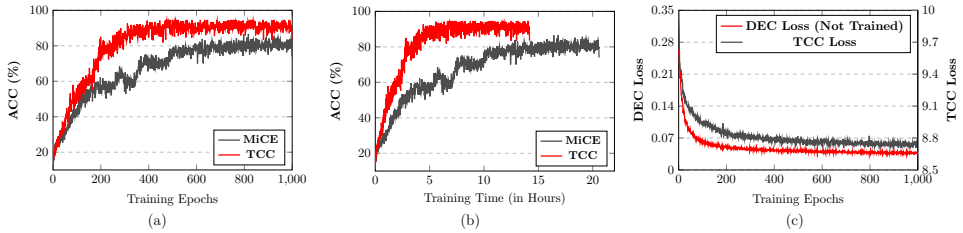


Figure 5: **(a) and (b):** On-batch ACC comparison between TCC and MiCE [73] *w.r.t.* training epochs and training time respectively on CIFAR-10 [44]. **(c)**: The values DEC loss [81] during training. Note that TCC is not trained with DEC, and we just record the figures for illustration.

essential role in the proposed model, having large values of α does not improve the performance, as the key instance-level semantics are yet learnt by $\mathcal{L}_2$. Only a reasonable proportion of $\mathcal{L}_1$, *e.g.*, $\alpha = 0.25$ or 0.5, in the overall learning objective improves the performance of our model. Further, we find that TCC is not very sensitive to the Gumbel softmax temperature λ, while a moderate hardness of the softmax produces the best results. Empirically, a large batch size benefits TCC, since more data can be involved in the subset of each cluster. Hence the aggregated features on each batch can be more representative. Fig. 4 (d) endorses this intuition. However, training with extremely large batch sizes may lead to out-of-memory problems with large images. To enable training on a single device, we opt to have a fixed batch size of $32 \times K$ in all experiments.

5.5 More Results

Training Time We compare the training epochs (Fig. 5 (a)) and training time (Fig. 5 (a)) of TCC and the re-implemented version of MiCE [73] with the same optimizer setting. As discussed in Sec. 3.3, MiCE obtains a higher time complexity during training than TCC. This is reflected in Fig. 5 (b), though not linearly proportional. In addition, TCC requires less training steps than MiCE to reach the best-performing results.

Conventional Clustering Losses During training, we also cache and observe the DEC loss [81], but we are **not** optimizing the model with it. In Fig. 5 (c), we show that by minimizing $\mathcal{L}$ (Eq. (9)), the traditional DEC loss [81] also decreases. This implicitly endorse our design.

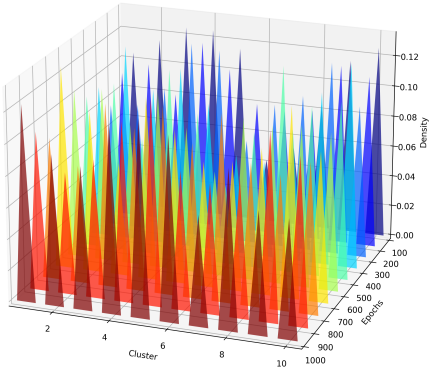


Figure 6: Histograms of cluster assignments during training on CIFAR-10 [44].

Assumptions in Design One merit of constrastive learning is that one does not need to assume any empirical prior distribution to the feature space, which benefits TCC when learning the cluster-level representations. The only assumption we employ is that the true posterior $p_\theta(k|\mathbf{x})$ should be uniform to simplify the computation of the KL-divergence in Eq. (6). As previously discussed, this conventional relaxation [69] is intuitively valid since we generally expect evenly assigned clusters. It is illustrated in Fig. 6 that TCC achieves this during training by minimizing $\mathrm{KL}\left(q_\theta(k|\mathbf{x})||p_\theta(k|\mathbf{x})\right) = -\log K - \mathcal{H}(q_\theta(k|\mathbf{x}))$.

6 Conclusion

Inspired by the recent success of self-supervised learning, this paper proposes a multi-granularity contrastive clustering framework to exploit the holistic context of a cluster in an unsupervised manner. The proposed TCC simultaneously learns instance- and cluster-level representations by leveraging cluster assignment variables. Cluster-level augmentation equivalents are derived to enable on-the-fly contrastive learning on clusters. Moreover, by reparametrizing the assignment variables, TCC can be trained end-to-end without auxiliary steps. Extensive experiments validate the superiority of TCC, which consistently outperforms competitors on the five benchmarks often by large margins, echoing our major motivation, *i.e.*, we are not clustering alone.

References

[1] Martín Abadi, Ashish Agarwal, Paul Barham, Eugene Brevdo, Zhifeng Chen, Craig Citro, Greg S Corrado, Andy Davis, Jeffrey Dean, Matthieu Devin, et al. Tensorflow: Large-scale machine learning on heterogeneous distributed systems. *arXiv:1603.04467*, 2016. 6

[2] Alexander A Alemi, Ian Fischer, Joshua V Dillon, and Kevin Murphy. Deep variational information bottleneck. In *International Conference on Learning Representations (ICLR)*, 2017. 6, 15

[3] Yoshua Bengio, Pascal Lamblin, Dan Popovici, Hugo Larochelle, et al. Greedy layer-wise training of deep networks. In *NeurIPS*, 2007. 7

[4] Christopher M Bishop. *Pattern recognition and machine learning*. springer, 2006. 1, 6

[5] Deng Cai, Xiaofei He, Xuanhui Wang, Hujun Bao, and Jiawei Han. Locality preserving nonnegative matrix factorization. In *IJCAI*, 2009. 7

[6] Mathilde Caron, Piotr Bojanowski, Armand Joulin, and Matthijs Douze. Deep clustering for unsupervised learning of visual features. In *ECCV*, 2018. 8

[7] Mathilde Caron, Ishan Misra, Julien Mairal, Priya Goyal, Piotr Bojanowski, and Armand Joulin. Unsupervised learning of visual features by contrasting cluster assignments. In *NeurIPS*, 2020. 6, 7, 14, 16

[8] Jianlong Chang, Yiwen Guo, Lingfeng Wang, Gaofeng Meng, Shiming Xiang, and Chunhong Pan. Deep discriminative clustering analysis. In *CVPR*, 2019. 7

[9] Jianlong Chang, Lingfeng Wang, Gaofeng Meng, Shiming Xiang, and Chunhong Pan. Deep adaptive image clustering. In *ICCV*, 2017. 6, 7

[10] Shlomo E Chazan, Sharon Gannot, and Jacob Goldberger. Deep clustering based on a mixture of autoencoders. In *MLSP*, 2019. 6

[11] Ting Chen, Simon Kornblith, Mohammad Norouzi, and Geoffrey Hinton. A simple framework for contrastive learning of visual representations. In *ICML*, 2020. 1, 2, 3, 4, 6, 7

[12] Xinlei Chen, Haoqi Fan, Ross Girshick, and Kaiming He. Improved baselines with momentum contrastive learning. *arXiv preprint arXiv:2003.04297*, 2020. 1, 2, 3, 6

[13] Yizong Cheng. Mean shift, mode seeking, and clustering. *IEEE Transactions on Pattern Analysis and Machine Intelligence*, 17(8):790–799, 1995. 6

[14] Adam Coates, Andrew Ng, and Honglak Lee. An analysis of single-layer networks in unsupervised feature learning. In *AISTATS*, 2011. 6, 7

[15] Luke Nicholas Darlow and Amos Storkey. Dhog: Deep hierarchical object grouping. *arXiv preprint arXiv:2003.08821*, 2020. 6, 7

[16] Nat Dilokthanakul, Pedro AM Mediano, Marta Garnelo, Matthew CH Lee, Hugh Salimbeni, Kai Arulkumaran, and Murray Shanahan. Deep unsupervised clustering with gaussian mixture variational autoencoders. *arXiv preprint arXiv:1611.02648*, 2016. 1, 6

[17] Harrison Edwards and Amos Storkey. Towards a neural statistician. In *ICML*, 2017. 6

[18] Martin Ester, Hans-Peter Kriegel, Jörg Sander, Xiaowei Xu, et al. A density-based algorithm for discovering clusters in large spatial databases with noise. In *SIGKDD*, 1996. 6

[19] Ji Feng and Zhi-Hua Zhou. Deep miml network. In *AAAI*, 2017. 6

[20] Brendan J Frey and Delbert Dueck. Clustering by passing messages between data points. *science*, 315(5814):972–976, 2007. 6

[21] Ian Goodfellow, Jean Pouget-Abadie, Mehdi Mirza, Bing Xu, David Warde-Farley, Sherjil Ozair, Aaron Courville, and Yoshua Bengio. Generative adversarial nets. In *NeurIPS*, 2014. 6, 7

[22] K Chidananda Gowda and G Krishna. Agglomerative clustering using the concept of mutual nearest neighbourhood. *Pattern recognition*, 10(2):105–112, 1978. 7

[23] Philip Haeusser, Johannes Plapp, Vladimir Golkov, Elie Aljalbout, and Daniel Cremers. Associative deep clustering: Training a classification network with no labels. In *German Conference on Pattern Recognition*, 2018. 6, 7

[24] Kaiming He, Haoqi Fan, Yuxin Wu, Saining Xie, and Ross Girshick. Momentum contrast for unsupervised visual representation learning. In *CVPR*, 2020. 1, 2, 3, 4, 5, 6, 8

[25] Kaiming He, Xiangyu Zhang, Shaoqing Ren, and Jian Sun. Deep residual learning for image recognition. In *CVPR*, 2016. 6

[26] Geoffrey Hinton, Oriol Vinyals, and Jeff Dean. Distilling the knowledge in a neural network. *arXiv preprint arXiv:1503.02531*, 2015. 2

[27] Weihua Hu, Takeru Miyato, Seiya Tokui, Eiichi Matsumoto, and Masashi Sugiyama. Learning discrete representations via information maximizing self-augmented training. In *ICML*, 2017. 6

[28] Jiabo Huang and Shaogang Gong. Deep clustering by semantic contrastive learning. *arXiv preprint arXiv:2103.02662*, 2021. 5, 6, 8

[29] Jiabo Huang, Shaogang Gong, and Xiatian Zhu. Deep semantic clustering by partition confidence maximisation. In *Proceedings of the IEEE/CVF Conference on Computer Vision and Pattern Recognition*, pages 8849–8858, 2020. 6, 7, 16

[30] Lawrence Hubert and Phipps Arabie. Comparing partitions. *Journal of classification*, 2(1):193–218, 1985. 6

[31] Maximilian Ilse, Jakub Tomczak, and Max Welling. Attention-based deep multiple instance learning. In *ICML*, 2018. 3, 6

[32] Eric Jang, Shixiang Gu, and Ben Poole. Categorical reparameterization with gumbel-softmax. In *ICLR*, 2017. 4, 5, 6, 8, 14

[33] Xu Ji, João F Henriques, and Andrea Vedaldi. Invariant information clustering for unsupervised image classification and segmentation. In *ICCV*, 2019. 6, 7, 8, 16

[34] Chao Jia, Yinfei Yang, Ye Xia, Yi-Ting Chen, Zarana Parekh, Hieu Pham, Quoc V Le, Yunhsuan Sung, Zhen Li, and Tom Duerig. Scaling up visual and vision-language representation learning with noisy text supervision. *arXiv preprint arXiv:2102.05918*, 2021. 1, 6

[35] Zhuxi Jiang, Yin Zheng, Huachun Tan, Bangsheng Tang, and Hanning Zhou. Variational deep embedding: An unsupervised and generative approach to clustering. *arXiv preprint arXiv:1611.05148*, 2016. 6

[36] Zhuxi Jiang, Yin Zheng, Huachun Tan, Bangsheng Tang, and Hanning Zhou. Variational deep embedding: An unsupervised and generative approach to clustering. In *IJCAI*, 2017. 1, 6, 7

[37] Hyunjik Kim, Andriy Mnih, Jonathan Schwarz, Marta Garnelo, Ali Eslami, Dan Rosenbaum, Oriol Vinyals, and Yee Whye Teh. Attentive neural processes. In *ICLR*, 2019. 6

[38] Diederik Kingma and Jimmy Ba. Adam: A method for stochastic optimization. In *ICLR*, 2015. 7

[39] Diederik Kingma and Max Welling. Auto-encoding variational bayes. In *ICLR*, 2014. 5, 6, 7, 14

[40] Diederik P Kingma, Shakir Mohamed, Danilo Jimenez Rezende, and Max Welling. Semi-supervised learning with deep generative models. In *NeurIPS*, 2014. 4, 5

[41] Alexander Kolesnikov, Xiaohua Zhai, and Lucas Beyer. Revisiting self-supervised visual representation learning. In *CVPR*, 2019. 6

[42] Andreas Kopf, Vincent Fortuin, Vignesh Ram Somnath, and Manfred Claassen. Mixture-of-experts variational autoencoder for clustering and generating from similarity-based representations. *arXiv preprint arXiv:1910.07763*, 2019. 6

[43] Hans-Peter Kriegel, Peer Kröger, Jörg Sander, and Arthur Zimek. Density-based clustering. *Wiley Interdisciplinary Reviews: Data Mining and Knowledge Discovery*, 1(3):231–240, 2011. 6

[44] Alex Krizhevsky and Geoffrey Hinton. Learning multiple layers of features from tiny images. *Technical Report, University of Toronto*, 2009. 6, 7, 8, 9

[45] Samuli Laine and Timo Aila. Temporal ensembling for semi-supervised learning. In *ICLR*, 2017. 4, 5, 14

[46] Ya Le and Xuan Yang. Tiny imagenet visual recognition challenge. *CS 231N*, 7(7):3, 2015. 7, 14, 16

[47] Yann LeCun, Yoshua Bengio, et al. Convolutional networks for images, speech, and time series. *The handbook of brain theory and neural networks*, 3361(10):1995, 1995. 3

[48] Yann LeCun, Léon Bottou, Yoshua Bengio, and Patrick Haffner. Gradient-based learning applied to document recognition. *Proceedings of the IEEE*, 86(11):2278–2324, 1998. 3

[49] Juho Lee, Yoonho Lee, Jungtaek Kim, Adam Kosiorek, Seungjin Choi, and Yee Whye Teh. Set transformer: A framework for attention-based permutation-invariant neural networks. In *ICML*, 2019. 3, 6, 15

[50] Juho Lee, Yoonho Lee, and Yee Whye Teh. Deep amortized clustering. *arXiv preprint arXiv:1909.13433*, 2019. 6

[51] Chongxuan Li, Max Welling, Jun Zhu, and Bo Zhang. Graphical generative adversarial networks. In *NeurIPS*, 2018. 6

[52] Junnan Li, Pan Zhou, Caiming Xiong, Richard Socher, and Steven CH Hoi. Prototypical contrastive learning of unsupervised representations. *arXiv preprint arXiv:2005.04966*, 2020. 6

[53] Yunfan Li, Peng Hu, Zitao Liu, Dezhong Peng, Joey Tianyi Zhou, and Xi Peng. Contrastive clustering. *arXiv preprint arXiv:2009.09687*, 2020. 5, 6, 7, 14, 15, 16

[54] Zhihan Li, Youjian Zhao, Haowen Xu, Wenxiao Chen, Shangqing Xu, Yilin Li, and Dan Pei. Unsupervised clustering through gaussian mixture variational autoencoder with non-reparameterized variational inference and std annealing. In *IJCNN*, 2020. 1

[55] Laurens van der Maaten and Geoffrey Hinton. Visualizing data using t-sne. *Journal of Machine Learning Research*, 9(Nov):2579–2605, 2008. 7

[56] James MacQueen et al. Some methods for classification and analysis of multivariate observations. In *Berkeley symposium on mathematical statistics and probability*, 1967. 1, 6, 8

[57] Chris J Maddison, Andriy Mnih, and Yee Whye Teh. The concrete distribution: A continuous relaxation of discrete random variables. In *ICLR*, 2017. 4, 5, 6, 8, 14

[58] Sudipto Mukherjee, Himanshu Asnani, Eugene Lin, and Sreeram Kannan. Clustergan: Latent space clustering in generative adversarial networks. In *AAAI*, 2019. 6

[59] Andrew Ng, Michael Jordan, and Yair Weiss. On spectral clustering: Analysis and an algorithm. In *NeurIPS*, 2001. 1, 6

[60] Chuang Niu and Ge Wang. Spice: Semantic pseudo-labeling for image clustering. *arXiv preprint arXiv:2103.09382*, 2021. 7

[61] Chuang Niu, Jun Zhang, Ge Wang, and Jimin Liang. Gatcluster: Self-supervised gaussian-attention network for image clustering. In *ECCV*, 2020. 6, 7, 16

[62] Aaron van den Oord, Yazhe Li, and Oriol Vinyals. Representation learning with contrastive predictive coding. *arXiv preprint arXiv:1807.03748*, 2018. 1, 2, 6

[63] Ari Pakman, Yueqi Wang, Catalin Mitelut, JinHyung Lee, and Liam Paninski. Neural clustering processes. In *ICML*, 2020. 6

[64] Sungwon Park, Sungwon Han, Sundong Kim, Danu Kim, Sungkyu Park, Seunghoon Hong, and Meeyoung Cha. Improving unsupervised image clustering with robust learning. *arXiv preprint arXiv:2012.11150*, 2020. 7

[65] Alec Radford, Luke Metz, and Soumith Chintala. Unsupervised representation learning with deep convolutional generative adversarial networks. In *ICLR*, 2016. 7

[66] Jayanth Reddy Regatti, Aniket Anand Deshmukh, Eren Manavoglu, and Urun Dogan. Consensus clustering with unsupervised representation learning. In *IJCNN*, 2021. 5, 14

[67] Olga Russakovsky, Jia Deng, Hao Su, Jonathan Krause, Sanjeev Satheesh, Sean Ma, Zhiheng Huang, Andrej Karpathy, Aditya Khosla, Michael Bernstein, et al. Imagenet large scale visual recognition challenge. *International Journal of Computer Vision*, 115(3):211–252, 2015. 6

[68] Guy Shiran and Daphna Weinshall. Multi-modal deep clustering: Unsupervised partitioning of images. In *ICPR*, 2021. 6, 7, 16

[69] Kihyuk Sohn, Honglak Lee, and Xinchen Yan. Learning structured output representation using deep conditional generative models. In *NeurIPS*, 2015. 4, 5, 9, 14

[70] Alexander Strehl and Joydeep Ghosh. Cluster ensembles—a knowledge reuse framework for combining multiple partitions. *Journal of machine learning research*, 3(Dec):583–617, 2002. 6

[71] Yaling Tao, Kentaro Takagi, and Kouta Nakata. Clustering-friendly representation learning via instance discrimination and feature decorrelation. In *ICLR*, 2021. 7, 14, 16

[72] Yonglong Tian, Dilip Krishnan, and Phillip Isola. Contrastive multiview coding. *arXiv preprint arXiv:1906.05849*, 2019. 6

[73] Tsung Wei Tsai, Chongxuan Li, and Jun Zhu. Mice: Mixture of contrastive experts for unsupervised image clustering. In *ICLR*, 2021. 1, 2, 5, 6, 7, 8, 9, 14, 15, 16

[74] Wouter Van Gansbeke, Simon Vandenhende, Stamatios Georgoulis, Marc Proesmans, and Luc Van Gool. Scan: Learning to classify images without labels. In *ECCV*, 2020. 6, 14

[75] Pascal Vincent, Hugo Larochelle, Isabelle Lajoie, Yoshua Bengio, Pierre-Antoine Manzagol, and Léon Bottou. Stacked denoising autoencoders: Learning useful representations in a deep network with a local denoising criterion. *Journal of machine learning research*, 11(12), 2010. 7

[76] Edward Wagstaff, Fabian Fuchs, Martin Engelcke, Ingmar Posner, and Michael A Osborne. On the limitations of representing functions on sets. In *ICML*, 2019. 6

[77] Jingyu Wang, Zhenyu Ma, Feiping Nie, and Xuelong Li. Progressive self-supervised clustering with novel category discovery. *IEEE Transactions on Cybernetics*, 2021. 6

[78] Joe H Ward Jr. Hierarchical grouping to optimize an objective function. *Journal of the American statistical association*, 58(301):236–244, 1963. 6

[79] Jianlong Wu, Keyu Long, Fei Wang, Chen Qian, Cheng Li, Zhouchen Lin, and Hongbin Zha. Deep comprehensive correlation mining for image clustering. In *ICCV*, 2019. 6, 7, 16

[80] Zhirong Wu, Yuanjun Xiong, Stella X Yu, and Dahua Lin. Unsupervised feature learning via non-parametric instance discrimination. In *CVPR*, 2018. 1, 2

[81] Junyuan Xie, Ross Girshick, and Ali Farhadi. Unsupervised deep embedding for clustering analysis. In *ICML*, 2016. 1, 6, 7, 9

[82] Yuwen Xiong, Mengye Ren, and Raquel Urtasun. Loco: Local contrastive representation learning. *arXiv preprint arXiv:2008.01342*, 2020. 6

[83] Bo Yang, Xiao Fu, Nicholas D Sidiropoulos, and Mingyi Hong. Towards k-means-friendly spaces: Simultaneous deep learning and clustering. In *ICML*, 2017. 6

[84] Bo Yang, Sen Wang, Andrew Markham, and Niki Trigoni. Robust attentional aggregation of deep feature sets for multi-view 3d reconstruction. *International Journal of Computer Vision*, 128(1):53–73, 2020. 6

[85] Jianwei Yang, Devi Parikh, and Dhruv Batra. Joint unsupervised learning of deep representations and image clusters. In *CVPR*, 2016. 6, 7

[86] Linxiao Yang, Ngai-Man Cheung, Jiaying Li, and Jun Fang. Deep clustering by gaussian mixture variational autoencoders with graph embedding. In *ICCV*, 2019. 1, 6

[87] Manzil Zaheer, Satwik Kottur, Siamak Ravanbakhsh, Barnabas Poczos, Russ R Salakhutdinov, and Alexander J Smola. Deep sets. In *NeurIPS*, 2017. 2, 5, 6, 15

[88] Matthew D Zeiler, Dilip Krishnan, Graham W Taylor, and Rob Fergus. Deconvolutional networks. In *CVPR*, 2010. 7

[89] Dejiao Zhang, Feng Nan, Xiaokai Wei, Shangwen Li, Henghui Zhu, Kathleen McKeown, Ramesh Nallapati, Andrew Arnold, and Bing Xiang. Supporting clustering with contrastive learning. In *NAACL*, 2021. 1, 6

[90] Dejiao Zhang, Yifan Sun, Brian Eriksson, and Laura Balzano. Deep unsupervised clustering using mixture of autoencoders. *arXiv preprint arXiv:1712.07788*, 2017. 6

[91] Tian Zhang, Raghu Ramakrishnan, and Miron Livny. Birch: an efficient data clustering method for very large databases. *SIGMOD*, 1996. 6

[92] Junjie Zhao, Donghuan Lu, Kai Ma, Yu Zhang, and Yefeng Zheng. Deep image clustering with category-style representation. In *ECCV*, 2020. 7

[93] Chengxu Zhuang, Alex Lin Zhai, and Daniel Yamins. Local aggregation for unsupervised learning of visual embeddings. In *ICCV*, 2019. 6

Summary of Revision

We introduce several additional unsupervised clustering articles, including [66, 71, 74].

We provide additional results on Tiny ImageNet [46] and comparison with more contrastive baselines such as SwAV [7] in Appendix D.

A The Instance-Level ELBO

Being not the main contribution of this paper, we are detailing our instance-level contrastive ELBO in the appendix to keep the main content concise. Here we reuse the inference model $q_\theta(k|\mathbf{x})$ as the pivot to bridge the cluster-level objective with the instance-level one. Similar to many VAE-like objectives [39], our ELBO can be derived with the Jensen's inequality $\log \mathbb{E}[\cdot] \geq \mathbb{E}[\log(\cdot)]$ as:

$$\begin{aligned}
\log p_\theta(i|\mathbf{x}) =& \log \sum_{k=1}^{K} p_\theta(i,k|\mathbf{x}) \\
=& \log \sum_{k=1}^{K} p_\theta(i|\mathbf{x},k) p_\theta(k|\mathbf{x}) \frac{q_\theta(k|\mathbf{x})}{q_\theta(k|\mathbf{x})} \\
=& \log \mathbb{E}_{q_\theta(k|\mathbf{x})} \left[p_\theta(i|\mathbf{x},k) \frac{p_\theta(k|\mathbf{x})}{q_\theta(k|\mathbf{x})} \right] \\
\geq& \mathbb{E}_{q_\theta(k|\mathbf{x})} \left[\log p_\theta(i|\mathbf{x},k) \right] + \mathbb{E}_{q_\theta(k|x)} \left[\log \frac{p_\theta(k|\mathbf{x})}{q_\theta(k|\mathbf{x})} \right] \\
=& \mathbb{E}_{q_\theta(k|\mathbf{x})} \left[\log p_\theta(i|\mathbf{x},k) \right] - \mathrm{KL}(q_\theta(k|\mathbf{x}) || p_\theta(k|\mathbf{x})) \\
=& \text{Eq. (6)}.
\end{aligned} \tag{10}$$

As discussed in the main body, the true distribution is $p_\theta(k|\mathbf{x})$ is unavailable in unsupervised learning. We use a uniform distribution as surrogate $p_\theta(k|\mathbf{x}) = p(k) = 1/K$. We also apply the Gumbel softmax trick [32, 57] as a relaxation to replace $\mathbb{E}_{q_\theta(k|\mathbf{x})}[\cdot]$. Thus, the gradients can be estimated by the reparametrization trick [39]. We write the full form of the final ELBO after relaxation as:

$$\mathbb{E}_\epsilon \left[\log p_\theta(i|\mathbf{x},\mathbf{c}) \right] - \mathrm{KL}(q_\theta(k|\mathbf{x}) || p(k)). \tag{11}$$

In our experiments, we sample a single Gumbel random variable ϵ for each image for TCC so that we can use a single-track memory bank for contrastive learning. This can be regarded as a stochastic layer added to the model for additional random augmentation. A similar spirit has been witnessed in [45] where a random noise model applies to enhance the robustness of the learnt representation. Sec. 5.4 shows that a one-sample solution obtains on-par performance as the multiple sampling baseline.

B Detailed Relations to Existing Models

We elaborate on the relations and differences between TCC and the most recent works [53, 73]. It is notable that we have discussed them in Sec. 3.4, and here provides more technical details. In addition, by the time of writing, [53] is yet a pre-print version.

B.1 MiCE [73]

We notice that [73] leverages a CVAE-like [69] lower-bound

$$\mathbb{E}_{q_\theta(k|\mathbf{x},i)} \left[\log p_\theta(i|\mathbf{x},k) \right] - \mathrm{KL}(q_\theta(k|\mathbf{x},i) || p_\theta(k|\mathbf{x})) \tag{12}$$

for instance-level contrast, and analytically computes the expectation term. Inference with MiCE yields a K-fold inference solution to obtain:

$$q_\theta(k|\mathbf{x},i) = \frac{p_\theta(k|\mathbf{x}) p_\theta(i|\mathbf{x},k)}{\sum_{k'=1}^{K} p_\theta(k'|\mathbf{x}) p_\theta(i|\mathbf{x},k')} \tag{13}$$

TCC derives a simpler version of instance-level contrast, and directly parametrizes the inference model $q_\theta(k|\mathbf{x})$ with neural networks. Note that the inference model in Eq. (3) directly describes a simple fully-connected layer with softmax activation. We show the complexity in Sec. 3.3.

On the other hand, MiCE does not consider cluster-level context learning, which counts the main contribution of this paper.

B.2 CC [53]

CC [53] introduces similar concepts as this paper in terms of **(1)** instance-level contrast with assignments and **(2)** literally 'cluster-level' contrast.

B.2.1 Instance-Level Objectives as VIB [2]

We firstly show the relation between TCC (proposed) and CC [53] in the instance-level objective with the help of variational information bottleneck (VIB) [2].

If we remove the dependency between the likelihood $p_\theta(i|\mathbf{x}, \mathbf{c})$ and $\mathbf{x}$, in Eq. (11) to have $p_\theta(i|\mathbf{x}, \mathbf{c}) \coloneqq p_\theta(i|\mathbf{c})$, the expectation of our instance-level ELBO becomes:

$$\mathbb{E}_{\mathbf{x}}\left[\mathbb{E}_\epsilon\left[\log p_\theta(i|\mathbf{c})\right] - \mathrm{KL}(q_\theta(k|\mathbf{x})||p(k))\right] \leq \mathcal{I}(I, C) - \mathcal{I}(C, X), \tag{14}$$

which is a special case of the ELBO of the information bottleneck $\mathcal{I}(I, C) - \beta\mathcal{I}(C, X)$ [2], with $\beta = 1$. CC [53] considers an even simpler deterministic version of this by removing the stochasticity. To this extent, the instance-level objective of CC can be regarded as a simplified version of our model.

The main difference here is whether we make the contrastive loss dependent on the image $\mathbf{x}$. We argue this dependency is of importance to inject discriminative information to identify each image. The category variables alone are not revealing the instance-level identities. This vision is also endorsed by MiCE [73]. In our experiments, we have shown that even without the cluster-level loss, TCC still obtains similar performance as CC [53] on CIFAR-10 (Sec. 5.4). Note that CC [53] comes with stronger random augmentations and is trained with larger image sizes. This result implicitly legitimates our instance-level design.

B.2.2 Cluster-Level Objectives and Representations

Literally, CC [53] involves a cluster-level contrastive learning process. Hence, we compare the cluster representations as follows:

$$\begin{aligned} \text{CC [53]: } \mathbf{r}_k &= [\pi_1(k), \cdots, \pi_B(k)] \\ \text{TCC (Ours): } \mathbf{r}_k &= \mathrm{L2Normalize}\left(\sum_{i=1}^{B} \pi_i(k) f_\theta(\mathbf{x}_i)\right). \end{aligned} \tag{15}$$

We use B to indicate the batch size. For CC [53], the degrees of relevance of the data in the batch to a cluster shape the corresponding representation. Note that this solution is not reflecting the latent semantics of a cluster, as reordering a batch would result in absolutely different vectors. The proposed TCC aggregates the features $f_\theta(\mathbf{x})$ according to the relevance $\pi(k)$ queried by the corresponding prototypes $\{\mu_k\}$. Reordering a batch does not change the content of the resulted $\mathbf{r}_k$. In Sec. 3.1, we have discussed that our aggregation is **semantically anchored** by the prototypes $\{\mu_k\}$. Though the actual values throughout different batches are slightly different, our cluster representations always reflect the same latent topics that are defined by $\{\mu_k\}$.

Our design is similar to *pooling by multihead attention* (PMA) in set transformer [49], which is also related to deep set representations [87]. The only difference here is that we are not normalizing the 'attention weights' $\pi_i(k)$ along the axis of i with softmax, as we are not expecting any datum to dominate the final cluster representation.

C CNN Backbone

Fig. 7 provides the details of the CNN backbone used in our experiments. All convolutional layers are followed by batch normalization and ReLU activation. Following [73], we disable the bias in the convolutional layers.

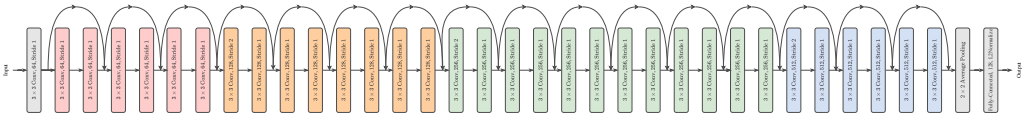


Figure 7: CNN backbone structure.

D More Results

D.1 Tiny ImageNet [46]

Table 4: Results on Tiny ImageNet [46] (in percentage %).

Method	NMI	ACC	ARI
DCCM [79]	22.4	10.8	3.8
CC [53]	34.0	14.0	7.1
TCC	43.5	30.6	15.2

We show the results on Tiny ImageNet [46] to illustrate the ability of TCC to recognize large numbers of clusters. Only some recent models are compared in Tab. 4 as there are not many articles that include this experiment.

D.2 More Contrastive Baselines

Table 5: Comparison with [7] on CIFAR-10 (in percentage %).

Method	NMI	ACC	ARI
DeepCluster-V2	65.2	72.7	58.9
SwAV [7]	71.1	79.6	64.9
TCC	79.0	90.6	73.3

We notice some pre-text contrastive learning models literally involve a clustering stage as a pre-training module to facilitate downstream tasks such as detection and segmentation, while we simply focus on a model dedicated to clustering. Comparing with them can be also interesting. We show the results with SwAV [7] in Tab. 5. We re-implement these baselines with the same CNN backbone as TCC, and train them at the same resolution as we described in the main body. It can be observed that these baselines obtain on-par performance against some recent methods. Though conceptually including clusters in training, they still mainly focus on better instance-level general representation learning, instead of improving the clustering assignments or preserving more cluster-level semantics.

D.3 Paired Hypothesis Testing

Table 6: Paired hypothesis test p-values

	IIC [33]	MMDC [68]	PICA [29]	GATCluster [61]	CC [53]	MoCo baseline [73]	MiCE [73]	IDFD [71]	TCC
IIC [33]		0.3213	0.0955	0.1895	0.01	0.0313	0.0048	0.0014	0.0005
MMDC [68]	0.3213		0.1649	0.4746	0.0105	0.1111	0.068	0.0228	0.0075
PICA [29]	0.0955	0.1649		0.024	0.0048	0.2876	0.1219	0.0046	0.0023
GATCluster [61]	0.1895	0.4746	0.024		0.0015	0.0551	0.0202	0.0003	0.0002
CC [53]	0.01	0.0105	0.0048	0.0015		0.0243	0.1843	0.2563	0.0191
MoCo baseline [73]	0.0313	0.1111	0.2876	0.0551	0.0243		0.0199	0.0456	0.0023
MiCE [73]	0.0048	0.068	0.1219	0.0202	0.1843	0.0199		0.121	0.0073
IDFD [71]	0.0014	0.0228	0.0046	0.0003	0.2563	0.0456	0.121		0.0778
TCC	0.0005	0.0075	0.0023	0.0002	0.0191	0.0023	0.0073	0.0778	

One of our reviewer suggests showing the performance significance against the existing models. Here we show the p-values of chi-squared test in Tab. 6.